LARGE-EDDY SIMULATIONS OF FLUID FLOW AND HEAT TRANSFER AROUND A PARABOLIC TROUGH SOLAR COLLECTOR

Ahmed Amine Hachicha, Ivette Rodríguez and Assensi Oliva[1]

[1]Heat and Mass Transfer Technological Center (CTTC)
Universitat Politècnica de Catalunya (UPC)
ETSEIAT, C. Colom 11, 08222 Terrassa (Barcelona), Spain
Fax: +34 93 739 89 20 e-mail: cttc@cttc.upc.edu

Abstract

This study reports on numerical simulations of a parabolic trough solar collector to predict the aerodynamic behaviour and the convection heat transfer from the heat collector element. In the study, the variation of fluid flow with different angles of attack has been taken into account. Calculations are performed using Large Eddy Simulations with a Variational Multiscale (VMS) approach for modelling the sub-grid scale stress tensor. The governing equations are discretised on a collocated unstructured grid arrangement by means of second-order spectro-consistent schemes. The numerical model is validated first with a cross flow around a horizontal cylinder. After that, aerodynamic coefficients at different angles of attack or pitch angles are calculated and compared to wind-tunnel experiments. It has been shown that, the orientation of the solar collector plays an important role in evaluating the aerodynamic performance and structural design criteria of the collector.

1. Introduction

Concentrated solar power plants are one of the most promising renewable options for electric generation. Parabolic trough collectors (PTC) are currently the most proven, widespread and commercially tested technology available for solar harnessing. PTC includes the parabolic reflector, the absorber tube with its associated glass cover, the metal support structure and the tracking system. The heat collector element (HCE) is the most important element in the system where the solar irradiation is absorbed and converted to thermal energy. In the case of forced convection (with winds), heat losses from the glass envelope are dominated mostly by convection.

The surrounding air is usually turbulent and can affect the optical performance and wind resistance of the PTC as well as the heat exchanges between the glass outer surface and the ambient air. Wind flow analysis is then required to understand the aerodynamic loading around the parabolic reflector as well as the convection heat transfer from the HCE. Hosoya and Peterka [1] have conducted a series of wind tunnel tests about a PTC with different configurations in which they included the peak load and the local pressure across the face of the solar collector and investigated the effect of Reynolds number on aerodynamic load coefficients. Current state-of-the-art for studying the flow around the parabolic collector and the absorber tube are based on resolving the time-averaged Navier-Stokes equations (RANS) [2, 3]. However, RANS methods suffer from inaccuracies in predictions of flow with massive separations. On the other hand, Large-Edddy Simulations (LES) methods have been proved to be more

suited for calculating these complex flows. The aim of this work is to simulate accurately the fluid flow and heat transfer around the PTC for different wind speed and pitch angles using a LES model.

2. Numerical Model

The parabolic collector is usually large in length and the aspect ratio of the HCE is very large, therefore wind flow can be assumed as two dimensional and the span-wise direction can be solved as a periodic flow. The methodology used for solving the fluid flow and heat transfer around the PTC is similar to that of bluff body flow described in Rodríguez et al .[4]. In this context, LES models have been proven to yield accurate results in flows with massive separations [5].

All the simulations are carried out using the CFD&HT code Termofluids [7], which is an unstructured and parallel object-oriented code for solving industrial flows. In Termofluids, the incompressible turbulent modelling of the Navier-Stockes equations are written as,

$$Mu = 0 \quad \text{(eq.1)}$$

$$\frac{\partial \overline{u}}{\partial t} + C(\overline{u})\overline{u} + \nu D\,\overline{u} + \rho^{-1} G\overline{p} - \bar{f} = C(\overline{u})\overline{u} - \overline{C(u)u} \approx -M\tau \quad \text{(eq. 2)}$$

$$\frac{\partial \overline{T}}{\partial t} + C(\overline{u})\overline{T} + \frac{\nu}{\mathrm{Pr}} D\,\overline{T} - \overline{\nabla \cdot q_{rad}} = C(\overline{u})\overline{T} - \overline{C(u)T} \approx -M\tau_T \quad \text{(eq. 3)}$$

where u , p ,T , t, $\bar{f}$, ν and ρ denote the velocity, pressure, temperature, time, body forces, kinematic viscosity and the air density respectively.

Convective and diffusive operators in the momentum equation for the velocity field are given by $C(u) = (u.\nabla)$, $D = -\nabla^2$. Gradient and divergence operators are given by $G = \nabla$ and $M = \nabla\cdot$, respectively. The last term in both equations indicates some modelisation of the filtered non-linear convective term. $\overline{u}$ and $\overline{T}$ are the filtered velocity and temperature, M represents the divergence operator of a tensor and τ is the SGS stress tensor which is defined as

$$\tau = -2\nu_{sgs}\overline{S} + \frac{1}{3}(\tau : \mathrm{I}) \quad \text{(eq. 4)}$$

where $\bar{S} = \frac{1}{2}[G(\overline{u}) + G^*(\overline{u})]$, where G^* is the transpose of the gradient operator. τ_T term is evaluated as in τ term, but ν_{sgs} is substituted by ν_{sgs}/Pr, where Pr is the turbulent Prandtl. In this work, the wall-adapting local-eddy viscosity (WALE) model within a Variational Multiscale approach [6] (VMS-WALE) is used for modelling the subgrid scale stress tensor.

In Termofluids, the governing equations are discretised on a collocated unstructured grid arrangement by means of second-order spectro-consistent schemes. Such schemes are conservative, i.e. they preserve the symmetry properties of the continuous differential operators and they ensure both, stability and conservation of the kinetic-energy balance even at high Reynolds numbers and with coarse grids. For the temporal discretisation of the momentum equation a two-steps linear explicit scheme on a fractional-step method is used for convective and diffusive terms, while for the pressure gradient term an implicit first-order scheme is used.

3. Results

The suitability for solving the flow around a PTC of the present numerical model is presented hereafter. First, the study of the fluid flow and heat transfer around a horizontal circular cylinder is analysed. Then, the study of the wind flow and aerodynamic coefficients around a PTC is performed. The results of both cases are compared against available experimental measurements from literature.

3.1. Fluid Flow and heat transfer around a horizontal circular cylinder

This case consists of a circular cylinder in cross flow. Two Reynolds numbers ($Re_D = \frac{uD}{\nu}$ where u is the free-stream velocity and D the cylinder diameter) are studied (7190 and 21580) and compared with experimental results of Scholten and Murray [9]. For both Reynolds numbers simulated Prandtl number ($Pr = \frac{\nu}{\alpha}$) is set at Pr=0.7. Cylinder wall temperature is set to 300K and free stream temperature is maintained at 350K. The boundary conditions at the inflow consist of uniform velocity and temperature. Slip and Neumann conditions are prescribed in the top and bottom boundaries of the domain for velocity and temperature, respectively. At the outlet, a pressure-based condition is used for momentum equation, whereas for energy equation a Neumann condition is assumed. At the cylinder surface, no-slip condition is prescribed for velocity.

The simulations are started from homogeneous flow and an impulsive flow initial condition is used. The flow field is advanced in time for initial duration to ensure temporal converged statistically. The time-averaged heat transfer results are computed over approximately (2000tu/D). The computational domain is extended to [-15D,25D];[-10D,10D];[0,πD] in the stream-, cross- and span-wise directions respectively, the cylinder is placed at (0,0,0). A three-dimensional mesh is generated by the constant-step extrusion of a two-dimensional unstructured grid. A prism mesh is used around the cylinder to well capture the boundary layer. The use of unstructured grid for the plane has allowed clustering more control volumes around the cylinder and in the near wake. The mesh is then stretched going away from the cylinder. Simulations are performed with two different grid resolutions by varying the number of control volumes (CVs) in the span-wise direction and around the circular cylinder. Two computational grids are considered: a coarse grid of 72000×32 planes (2.3MCVs) and a finer grid of 130000×64 planes (8.3MCVs).

First, the distribution of the drag forces around the circumference of the cylinder for both grids at $Re_D = 7190$ is calculated and compared with experimental measurements of Norberg [11]. Figure 1 shows the results on both meshes together with the experimental data by Norberg [11] at $Re_D = 8000$. Both grids capture the pressure distribution in the laminar zone reasonably well. However, the low-resolution mesh over-predicts the pressure in the back zone and the magnitude of the minimum pressure on the cylinder surface. On the other hand, the high-resolution mesh reproduces accurately the experimental results of Norberg [11] with the same minimum magnitude and angle position where it occurs.

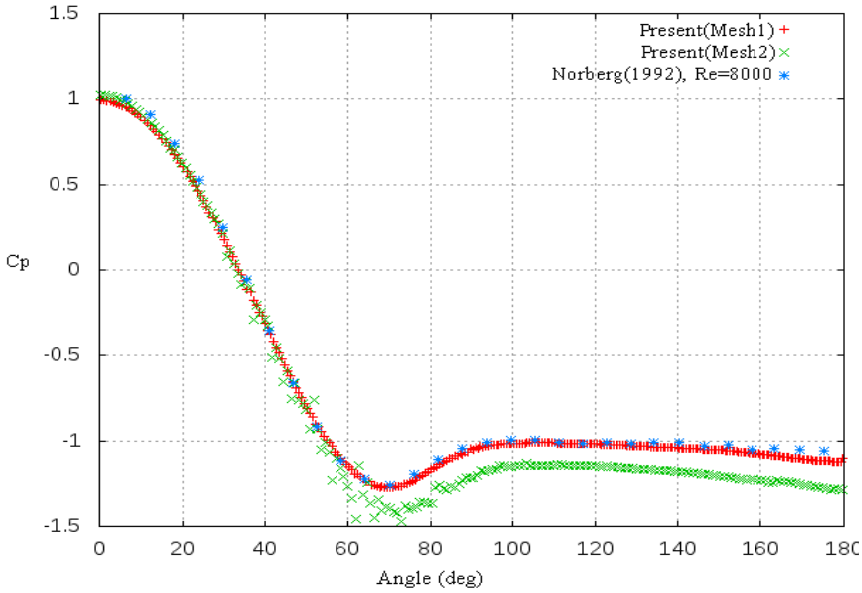

Fig.1. Variation of the drag coefficient around the cylinder for two grid resolutions. Comparison with experimental data of Norberg [11].

For the finer grid, which predicts well the flow dynamics and drag forces in the cylinder surface, the Nusselt number is evaluated. The Nusselt number ($Nu=hD/\lambda$) which describes the heat transfer characteristics for the flow around the bluff body is calculated around the circumference of the cylinder. The calculated local Nusselt number gives a good agreement with experimental measurements [9] and follows the same trends as shown in Figure 2. The Nusselt number is maximum at the leading edge or the front stagnation point (fsp) and decreases smoothly by moving towards the top (or the bottom) of the cylinder. The minimum value occurs at about 90º from the stagnation point of the cylinder which is associated with flow separation and the formation of a recirculation zone in the near wake. That is, the local separation restricts heat transfer away from the surface and causes the decrease of the Nusselt number. It increases again by approaching to the wake region as the turbulent wake allows heat to again be removed.

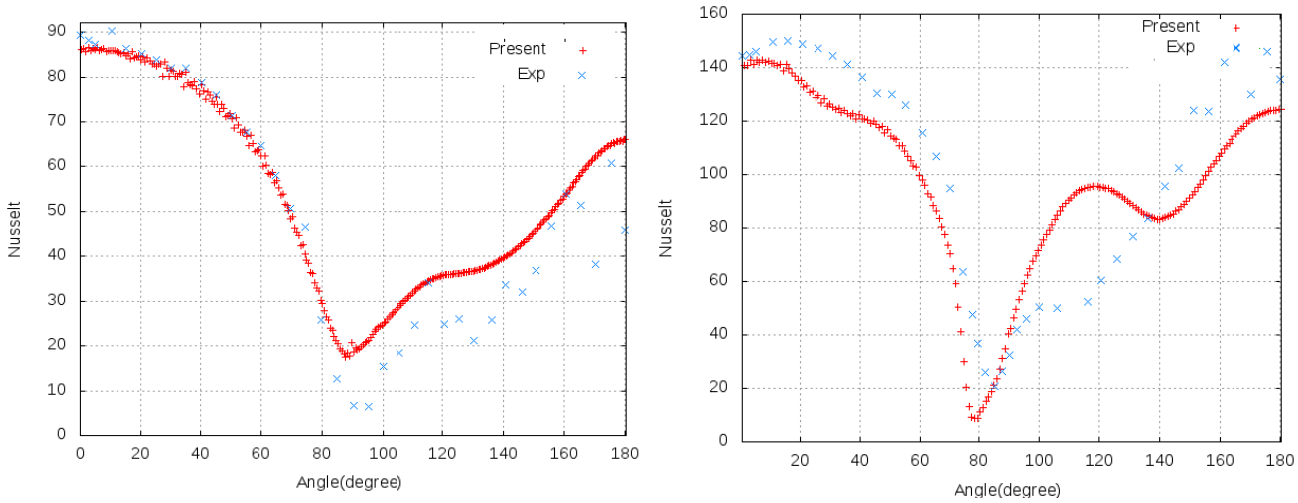

(a) (b)

Fig. 2. Variation of the Nusselt number around the cross flow horizontal cylinder and comparison with experimental data at (a) Re=7190 and (b) Re=21580 [9].

The numerical results of the averaged Nusselt number and the front stagnation point Nusselt number are summarized in Table 1 for both cases and compared with experimental measurements [9] and the correlation of Zukasuskas [10] for the mean Nusselt number of a single cylinder in low turbulence and low blockage cross flow.

Table 1. Comparison of front stagnation point and average Nusselt number with experiments [9] and values obtained by Zukasuskas correlation [10].

Re	Nu_{fsp}	Nu_{fsp} (exp)	%error (exp)	Nu_{avg}	Nu_{avg} (Zukasuskas)	Nu_{avg}(exp)	%error (exp)
7190	86.58	88	1.6	52.22	47.3	49.5	5.49
21580	147.68	148	0.2	96.86	91.3	103.4	6.32

3.2. Wind Flow around a parabolic trough solar collector

The wind flow and heat transfer is also studied around a typical LS-2 parabolic trough solar collector [8]. The numerical model is validated with wind-tunnel experiments [1] conducted on a LS-2 PTC [8] in the same range of Reynolds numbers ($Re_W = 2 \times 10^6$) based on the aperture of the parabola (W=5m). The computational domain is defined by 5W in the upstream direction, 20W in the downstream direction, 9 W in the cross direction and πW in the span-wise direction. A constant wind speed (u_∞=7 m/s) is considered in the inlet boundary condition. Slip conditions are fixed in the top and bottom boundaries, while at the outlet a pressure-based condition is used. At the mirror and HCE surfaces, no-slip conditions are prescribed. As for the span-wise direction, periodic boundary conditions are imposed. In a similar manner to section 3.1 a three dimensional extruded mesh is generated. The mesh is refined around the mirror, the HCE and the near wake and then stretched going away from the collector.

Extensive grid refinement tests for each pitch angle are conducted in order to obtain a solution which accurately describes the fluid flow and heat transfer phenomena. For the sake of brevity, these studies are not shown and only results obtained with the finer grid for each pitch angle are presented. Indeed, finer meshes are about 7 MCVs with 96 planes in the homogenous direction. Aerodynamic coefficients at different pitch angles are calculated and compared to experimental measurements in Figure 4. As can be seen from the figure, numerical results obtained by the present model are within the error-bars of both experimental measurements from the wind-tunnel data [1]. The discrepancies between predicted and measured aerodynamic coefficient are most likely due to the unsteady flow behaviour and the ground effect. On the other hand, there also could be some differences with the experiments due to the wide range of Reynolds number adopted in the model-to-full-scale test.

The zero pitch angle presents the maximum horizontal drag force (C_P) and it decreases by moving the parabolic trough toward the horizontal position. However, the lift coefficient (C_f) increases by approaching to the stow mode where the concave surface of the trough is facing the ground.

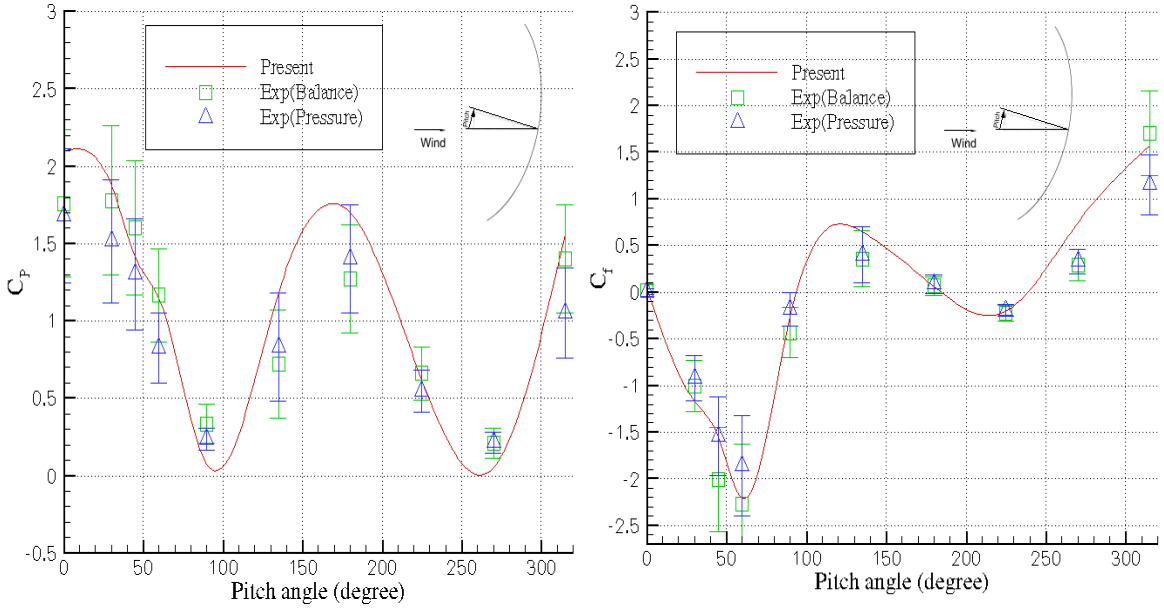

(a) (b)

Fig. 4. Predicted and measured aerodynamic parameters for LS-2 PTC. (a) drag and (b) lift coefficients.

The variations of the aerodynamic coefficients can clearly be understood if the instantaneous flow is studied. In figure 5, the instantaneous velocity field for different pitch angles (θ=0º, θ=45º and θ=90º) are depicted. A large separated zone is observed at θ=0º. The turbulent flow in the detached region produces a large depression region in the back of the PTC being the responsible for the large value of drag coefficient obtained. With the increase of the pitch angle from θ=0º to θ=90º the separated zone is continuously reduced which provokes the reduction of drag forces in the PTC surface.

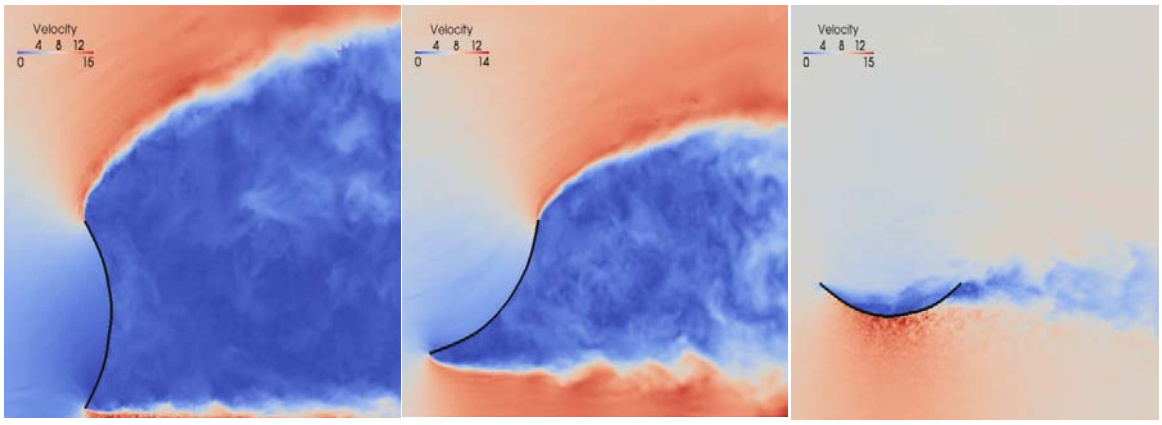

(a) (b) (c)

Fig. 5. Instantaneous velocities around the PTC for different pitch angles: (a) θ=0º, (b) θ=45º and (c) θ=90º

Numerical simulations are also carried out to study the heat transfer from the HCE of the LS-2 PTC. The temperatures of the glass cover and ambient air are fixed to 300 K and 350 K respectively. The parabolic mirror is oriented to the horizontal position (θ=90º), which corresponds to the normal operation mode. The Reynolds number based on the glass cover diameter is about 22320 which is alike

to the Reynolds number considered in the validation of cross flow around horizontal cylinder (see section 3.1). The comparisons show that the Nusselt number for cross flow around a horizontal cylinder is higher than the Nusselt number for wind flow around a HCE of a PTC. This reduction is desirable, since it reduces heat losses from the HCE and improves the thermal efficiency. The minimum of Nusselt number is displaced away the stagnation point and occurs at about 85º. After reaching the local minimum, the increase of Nu in the wake zone is smoother.

In general, the circumferential variation of the Nusselt number in the case of the HCE is similar to the simple cross flow and the effect of the parabolic mirror can be seen mainly in the reduction of the magnitude of Nusselt number.

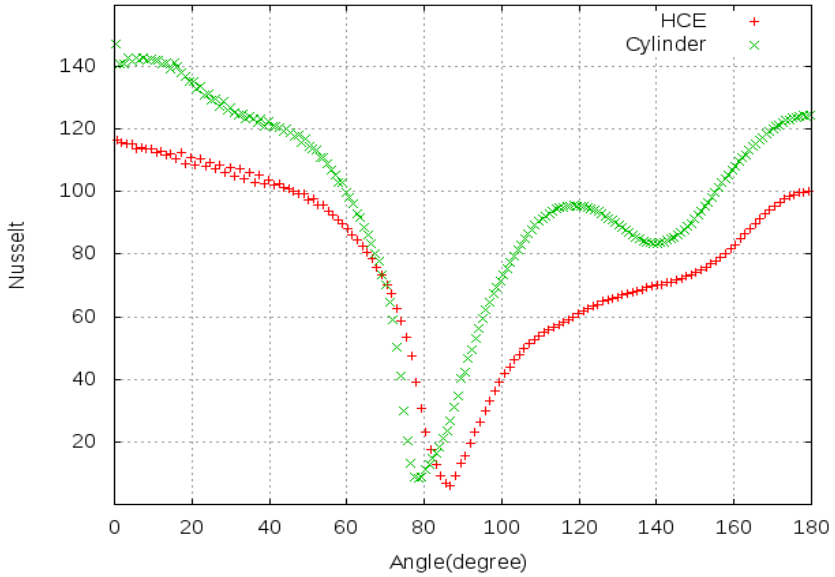

Fig. 3. Comparison of the Nusselt number around the HCE and the cross flow horizontal cylinder.

4. Conclusions

A study of fluid flow and heat transfer around the HCE and the PTC has been carried out by means of large-eddy simulations. The suitability of the model used for accurate predicting the flow dynamics and heat transfer present is analysed by comparing the results with experimental measurements. Present simulations proved to reproduce accurately the aerodynamic and thermal behaviour around PTC under turbulent wind flow conditions. Aerodynamic coefficients are calculated for different pitch angles and give good agreements with the experiments measurements. The drag force is maximum when the wind blows normal to the concave of the parabolic mirror and minimum when the collector is oriented parallel with wind direction. The lift force is more important in the stow mode than in the normal mode. In addition, the influence of the parabola on the heat transfer in the HCE is also analysed by comparing the results with those obtained from a circular cylinder in cross-flow. Results shown that the magnitude of the Nusselt number decreases with the presence of the parabolic mirror and tend to be smoother.

Further work is ongoing to determine the effect of the pitch angle on the Nusselt number as well as the effect of Reynolds number on the fluid flow around the solar collector.

Acknowledgments

This work has been partially financially supported by the "Ministerio de Economía y Competitividad, Secretaría de Estado de Investigación, Desarrollo y Innovación" Spain (ref. ENE2010-17801), and by the "Agencia Española de Cooperación Internacional para el Desarrollo" (AECID).

References

[1] N. Hosoya, J.A. Peterka, R.C. Gee, D. Kearney. Wind tunnel tests of parabolic trough solar collectors March 2001-August 2003, NREL/SR Report 550-32282 (2008).

[2] N. Naeeni, M. Yaghoubi. Analysis of wind flow around a parabolic collector (1) fluid flow Renewable Energy, 32 (2007), pp. 1898–1916.

[3] N. Naeeni, M. Yaghoubi. Analysis of wind flow around a parabolic collector (2) fluid flow Renewable Energy, 32 (2007), pp. 1259-1272.

[4] I. Rodríguez, R. Borrell, O. Lehmkuhl, C.D. Pérez-Segarra & A. Oliva. Direct numerical simulation of the flow over a sphere at re = 3700. Journal of Fluids Mechanics 679 (2011) 263-287 .

[5] O. Lehmkuhl, A. Baez, I. Rodríguez and C.D. Pérez-Segarra. DNS and LES of the turbulent flow around a NACA-0012 airfoil. In ICCHMT 7. Turkey (2011).

[6] T.J.R. Hughes, L. Mazzei & K.E. Jansen. Large eddy simulation and the variational multiscale method. Computing and Visualization in Science, 3 (2000) 47-59.

[7] O. Lehmkuhl, R. Borell, C.D. Pérez-Segarra, M. Soria, A. Oliva, 2007. A new parallel unstructured CFD code for the simulation of turbulent industrial problems on low cost PC CVluster, Proceedings op PCFD, Turkey.

[8]Cohen, G.E., D.W. Kearney and G.J. Kolb (1999), Final Report on the Operation and Maintenance Improvement for Concentrating Solar Power Plants, Report SAND99-1290, Sandia National Laboratories.

[9] J. W. Scholten and D. B. Murray, Unsteady Heat Transfer and Velocity of a Cylinder in Cross Flow- I. Low Freestream Turbulence, Int. J. of Heat and Mass Transfer, 1998, 41, (10), 1139–1148.

[10] Zukauskas, A., Heat transfer from tubes in cross flow. Advances in Heat Transfer, 1972, 8, 93-160.

[11] Norberg, C. 1993 Pressure forces on a circular cylinder in cross flow. In Bluff Body Wakes, Dynamics and Instabilities (ed. H. Eckelmann, J. M. Graham. P. Huerre & P. A Monkewitz), Proc. IUTAM Symp. 115, 7–11 September 1992, GÂ¨gttingen. Springer.